Study of the process $e^+e^- \to \pi^+\pi^-\pi^0\eta$ at the SND detector

A.A.Botov[1],[⋆]

[1]*Budker Institute of Nuclear Physics, Novosibirsk, 630090, Russia*

Abstract. The reaction $e^+e^- \to \pi^+\pi^-\pi^0\eta$ has been studied in the experiment with the SND detector at the VEPP-2000 e^+e^- collider. The reaction proceeds via the four intermediate states: $\omega\eta$, $\phi\eta$, $a_0\rho$, and structureless $\pi^+\pi^-\pi^0\eta$ state, which may be, for example, $\rho(1450)$ with $\rho(1450) \to \rho(770)\eta$. The total $e^+e^- \to \pi^+\pi^-\pi^0\eta$ cross section and cross section for the four intermediate states have been measured and fitted in the vector meson dominance model.

1 Introduction

The main goal of experiments with the SND detector at the VEPP-2000 e^+e^- collider is precision measurement of the total cross section of e^+e^- annihilation to the hadrons in the center-of-mass (c.m.) energy region below 2 GeV. The total cross section is necessary for calculation of the running electromagnetic coupling constant and the muon anomalous magnetic moment. Below 2 GeV the total hadronic cross section is calculated as a sum of exclusive cross sections for all possible hadronic modes. The process $e^+e^- \to \pi^+\pi^-\pi^0\eta$ gives a sizeable contribution to the total cross section above 1.6 GeV. It was established [1] that the $e^+e^- \to \pi^+\pi^-\pi^0\eta$ reaction proceeds through $\omega\eta$, $\phi\eta$, $\rho a_0(980)$ intermediate states and a structureless $\pi^+\pi^-\pi^0\eta$ mechanism. The latter may be, for example, $rho(1450)\pi$ with $\rho(1450) \to \rho(770)\eta$ decay. The cross sections for $e^+e^- \to \omega\eta$ and $\phi\eta$ were previously measured in several final states [2–4]. The only measurement of the $e^+e^- \to \pi^+\pi^-\pi^0\eta$ reaction was performed very recently in the CMD-3 experiment [5] also at VEPP-2000.

This work is dedicated to the measurement of the $e^+e^- \to \pi^+\pi^-\pi^0\eta$ cross section at the SND detector. We analyze the $\pi^+\pi^-\pi^0\eta$ final state with the η meson decayed to $\gamma\gamma$.

SND [6] is a general purpose nonmagnetic detector. The main part of SND is a spherical three-layer electromagnetic calorimeter containing 1640 NaI(Tl) crystals and covering a solid angle of 95% of 4π. Directions of charged particles are measured by a tracking system based on a nine-layer cylindrical drift chamber and a proportional chamber with cathode-strip readout in a common gas volume. The tracking system covers a solid angle of 94% of 4π. The particle identification is provided by dE/dx measurements in the tracking system and a system of aerogel Cherenkov counters. Outside the calorimeter a muon detector is located.

SND collected data at the VEPP2000 [7] e^+e^- collider operating in the c.m. energy region 0.3–2.0 GeV. A 69 pb^{-1} data sample was collected during 2010–2013. At the end of 2016 year, after finishing of upgrade, VEPP2000 resumed operation. About 50 pb^{-1} of integrated luminosity has been accumulated during 2017 data taking run.

[⋆]e-mail: A.A.Botov@inp.nsk.su

2 Data and simulation

This analysis is based on data with an integrated luminosity of 27 pb^{-1} recorded with the SND detector in 2011–2012 in 36 energy points of the range 1.34–2 GeV, above the threshold of the process under study. Experimental energy points are merged into 13 energy intervals with 50 MeV width.

Simulation of the signal and background processes is done with Monte Carlo (MC) event generators. The generators take into account radiative corrections to the initial particles calculated according to Ref. [8]. The cross-section energy dependences needed for radiative-correction calculation are taken from existing data, e.g., from Ref. [2] for the process $e^+e^- \to \omega\eta$. For the processes $e^+e^- \to a_0\rho$ and structureless mechanism of the $e^+e^- \to \pi^+\pi^-\pi^0\eta$ reaction, we use cross sections from our measurements through iterations. For simulation of the structureless mechanism the hypothesis $e^+e^- \to \rho(1450)\pi$ with $\rho(1450) \to \rho(770)\eta$ is used.

Interactions of generated particles with the detector material are simulated using GEANT4 software [9]. The simulation takes into account variation of experimental conditions during data taking, in particular dead detector channels and beam-induced background.

The luminosity is measured using the process of Bhabha scattering $e^+e^- \to e^+e^-$. The detection efficiency and cross section for Bhabha events are determined using the event generator BH-WIDE [10]. The systematic uncertainty of the luminosity measurement does not exceed 2%.

3 Event selection

The following preselection is used. There are two or three charged particles originated from the interaction region and at least four photons with energy greater than 20 MeV in an event. The total energy deposition in the calorimeter for these events is required to be greater than 300 MeV.

For preliminary selected events the vertex fit characterized by the parameter χ_r^2 is performed using the parameters of two charged tracks. If there are three charged tracks in an event, the two tracks with the lowest χ_r^2 value are selected. The found vertex is used to refine the measured angles of charged particles and photons. Then, a kinematic fit to the $e^+e^- \to \pi^+\pi^-\pi^0\gamma\gamma$ hypothesis characterized by the parameter $\chi_{3\pi2\gamma}^2$ is performed with the requirement of energy and momentum balance and the invariant mass of the π^0 candidate constrained to its world average value [11]. The fit uses the measured polar and azimuthal angles of charged particles, and the measured angles and energies of photons. The invariant mass of the photon pair, which are assumed to be the η-meson candidate, must be in the range $400 < M_{\gamma\gamma} < 700$ MeV. All possible combinations of photons are tested and the combination with the smallest $\chi_{3\pi2\gamma}^2$ is chosen. The photon parameters after the kinematic fit are used to recalculate the η-candidate invariant mass (M_η). The event is then refitted with the η-mass constraint. The refined η-candidate energy is used to calculate the invariant mass of the system recoiling against the η meson (M_η^{rec}).

Events of the process under study are selected by the conditions $\chi_{3\pi2\gamma}^2 < 30$. To suppress background from the process $e^+e^- \to \pi^+\pi^-\pi^0\pi^0$ we perform a kinematic fit to the hypothesis $e^+e^- \to \pi^+\pi^-\pi^0\pi^0(\gamma)$ (radiation of an additional photon along the beam axis is allowed) and reject events with $\chi_{4\pi(\gamma)}^2 < 200$.

The $\chi_{3\pi2\gamma}^2$ distribution for selected data events is shown in Fig. 1 in comparison with the simulated distributions for signal and background $e^+e^- \to \pi^+\pi^-\pi^0\pi^0$ events. The signal peak near zero is clearly seen in the distribution. However, the region $\chi_{3\pi2\gamma}^2 < 30$ contains a significant amount of background events.
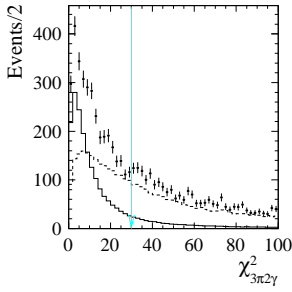
Figure 1. The $\chi^2_{3\pi2\gamma}$ distribution for selected data events (points with error bars). The solid and dashed histograms represent the shapes of signal and background $e^+e^- \rightarrow \pi^+\pi^-\pi^0\pi^0$ distributions obtained using MC simulation, respectively. The arrow indicates the boundary of the condition $\chi^2_{3\pi2\gamma} < 30$.
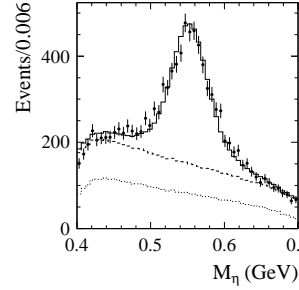
Figure 2. The spectrum of the two-photon invariant mass of the η-meson candidate for selected data events (points with error bars). The solid histogram is the result of the fit to the data spectrum with a sum of signal and background distributions. The background distribution is shown by the dashed histogram. The dotted histogram represents the $e^+e^- \rightarrow \pi^+\pi^-\pi^0\pi^0$ background contribution.

4 Determination of the number of signal events

The M_η spectrum for selected data events is shown in Fig. 2. To extract the number of signal $e^+e^- \rightarrow \pi^+\pi^-\pi^0\eta$ events the spectrum is fitted with a sum of signal and background distributions. The background distribution is a sum of the simulated distribution for $e^+e^- \rightarrow \pi^+\pi^-\pi^0\pi^0$ and a linear function. The signal distribution is described by a sum of three Gaussian distributions with parameters determined from the fit to the simulated M_η distribution for $e^+e^- \rightarrow \pi^+\pi^-\pi^0\eta$ events.

The distributions of the signal events for invariant mass M_η^{rec} for different c.m. energy intervals are shown in Fig. 3. The ω- and ϕ-meson peaks are clearly seen. We define contributions of the intermediate states through approximation of these spectra with a sum of simulated distributions for them. To clear $a_0\rho$ contribution for energies greater than 1.694 GeV we use simultaneous approximation of the three distributions for M_η^{rec}, $M_{\pi^0\eta}$ and $M_{\pi^\pm\eta}$ also shown in Fig. 3. The a_0 peaks are seen in the latter two distributions.

For $\omega\eta$ and $\phi\eta$ channels we use three Gaussian distributions with parameters determined from the fit to the simulated distributions. For the $a_0\rho$ and structureless $e^+e^- \rightarrow \pi^+\pi^-\pi^0\eta$ decay channels simulated histograms are used.

5 The Born cross section

The experimental values of the each visible cross section are calculated as follows,

$$\sigma_{vis,i} = \frac{N_i}{L_i\varepsilon_i B},$$

(1)

where N_i, L_i, and ε_i are the number of selected data events, integrated luminosity, and detection efficiency for the i-th energy interval shown in Fig. 4, and B is the branching fraction of decay to the $\pi^+\pi^-\pi^0\eta$ final state which for the $\omega\eta$ and $\phi\eta$ channels are taken from Particle Data Group (PDG) [11] and for the rest two are equal to unit. For the total cross section we calculated N_i/ε_i as the following,

$$\frac{N}{\varepsilon} = \frac{N_{\omega\eta}}{\varepsilon_{\omega\eta}} + \frac{N_{\phi\eta}}{\varepsilon_{\phi\eta}} + \frac{N_{a_0\rho}}{\varepsilon_{a_0\rho}} + \frac{N_{nres}}{\varepsilon_{nres}}.$$

(2)

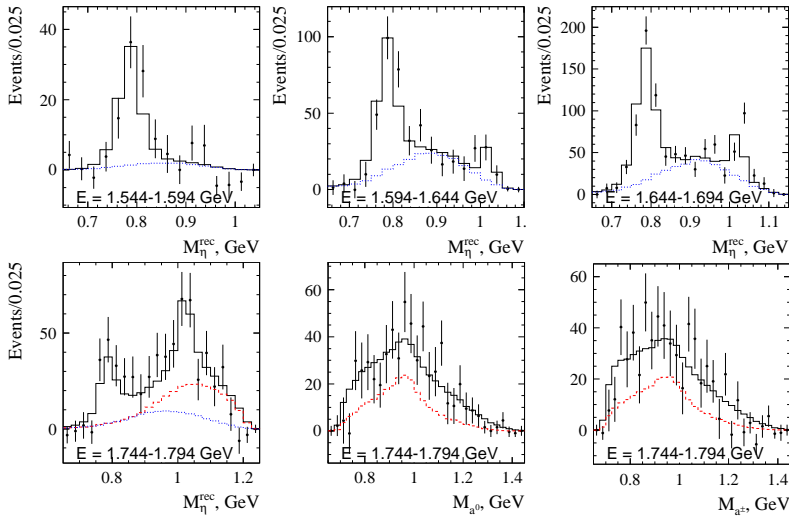**Figure 3.** The M_η^{rec} distribution for data $e^+e^- \to \pi^+\pi^-\pi^0\eta$ events from different c.m. energy intervals (points with error bars). The solid histogram represents the result of the fit described in the text. The dotted histogram represents the structureless $e^+e^- \to \pi^+\pi^-\pi^0\eta$ contribution. The dashed histogram represents the $e^+e^- \to a_0\rho$ contribution.
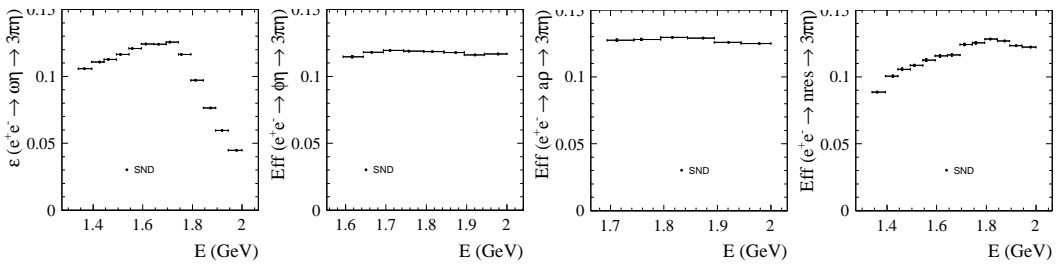

Figure 4. The detection efficiencies for the four studied channels.

The visible cross section is related to the Born cross section (σ) by the following expression [8]:

$$\sigma_{vis}(E) = \int_0^{x_{max}} F(x, E)\sigma(E\sqrt{1-x})dx, \qquad (3)$$

where the function $F(x, E)$ describes the probability of radiation of photons with total energy $xE/2$ by the initial electron and positron, and $x_{max} = 1 - (2m_{\pi^+} + m_{\pi^0} + m_\eta)^2/E^2$. The right side of Eq. (3) can be rewritten in the more conventional form,

$$\int_0^{x_{max}} F(x, E)\sigma(E\sqrt{1-x})dx = \sigma(E)(1 + \delta(E)), \qquad (4)$$

where $\delta(E)$ is the radiative correction.

Experimental values of the Born cross section are determined as follows. The energy dependence of the measured visible cross section is fitted with Eq. (3), in which the Born cross section is given by a theoretical model describing data well. The model parameters obtained in the fit are used to calculate $\delta(\overline{E}_i)$, where $\overline{E}_i$ is the weighted average c.m. energy for ith energy interval, defined in Sec. 2. The values of the Born cross section are then obtained as $\sigma_i = \sigma_{vis,i}/(1 + \delta(\overline{E}_i))$.

For the $\omega\eta$ and structureless $\pi^+\pi^-\pi^0\eta$ channels the Born cross section is described by a sum of two resonance contributions,

$$\sigma(E) = \frac{12\pi}{E^3} \left| \sqrt{\frac{B_{\omega'}}{P_f(m_{\omega'})}} \frac{m_{\omega'}^{3/2}\Gamma_{\omega'}}{D_{\omega'}} - \sqrt{\frac{B_{\omega''}}{P_f(m_{\omega''})}} \frac{m_{\omega''}^{3/2}\Gamma_{\omega''}}{D_{\omega''}} \right|^2 P_f(E), \qquad (5)$$

where $B_V = B(V \to e^+e^-)B(V \to f)$ is the product of the branching fractions for the V decay to e^+e^- and f, where $f = \omega\eta$ and $f = \pi^+\pi^-\pi^0\eta$ for $\omega\eta$ and structureless channels correspondingly, $D_V = E^2 - m_V^2 + iE\Gamma_V$, m_V and Γ_V are the mass and width of the resonance V ($V = \omega'$ or ω''). The phase space factor $P_f(E)$ is given by

$$P_f(E) = q(E)^3, \quad q(E) = q(E, m_\omega, m_\eta) = \frac{1}{2E}\sqrt{(E^2 - (m_\omega - m_\eta)^2)(E^2 - (m_\omega + m_\eta)^2)} \qquad (6)$$

for the $\omega\eta$ and unit for structureless channel correspondingly. The first term in Eq. (5) describes the $\omega(1420)$ contribution. The second term is a sum of contributions of the $\omega(1650)$ and $\phi(1680)$ resonances. The phase between the first and second terms is chosen to be equal to π (see the discussion below).

For the $\phi\eta$ and $a_0\rho$ channels we use one resonance V, which is ϕ' for the first one. For the first one the phase space factor $P_f(E)$ is given by

$$P_f(E) = q(E)^3, \quad q(E) = \frac{1}{2E}\sqrt{(E^2 - (m_\phi - m_\eta)^2)(E^2 - (m_\phi + m_\eta)^2)} \qquad (7)$$

and for the second one is given by

$$P_f(E) = \frac{1}{3}q_f \cdot \frac{2}{3} = \frac{2}{9} \int_{4m_\pi^2}^{(E-m_{a_0})^2} \frac{dm^2}{\pi} \frac{m\Gamma_\rho(m)q(E, m, m_{a_0})}{(m^2 - m_\rho^2)^2 + m^2\Gamma_\rho^2(m)},$$

$$\Gamma_\rho(m) = \Gamma_\rho \frac{m_\rho^2}{m^2}\left(\frac{p_\pi^2(m^2)}{p_\pi^2(m_\rho^2)}\right)^{3/2}, \quad p_\pi^2(m^2) = m^2/4 - m_\pi^2, \qquad (8)$$

For the total cross section we used two resonances with a free phase between them.

The free fit parameters are $B_{\omega'}$, $B_{\omega''}$, $B_{\phi'}$, $m_{\omega''}$, $\Gamma_{\omega''}$. The mass and width of the $\omega(1420)$ resonance are fixed at their PDG values [11]. The fit performed with zero phase between the ω' and ω'' amplitudes provides a significantly worse ($\chi^2 = 41.6$) description of the cross-section data. The fitted curves together with obtained values of the Born cross sections are shown in Fig. 5.

The contribution of the $\omega(1420)$ is small compared with that of the ω''. However, this contribution is necessary to describe the asymmetry of the peak in the measured cross section. The asymmetry is explained by constructive interference of the ω' and ω'' amplitudes on the left side of the peak and destructive interference on the right side.

6 Conclusions

In this paper we present the analysis of the process $e^+e^- \to \pi^+\pi^-\pi^0\eta$ made with the SND detector at the VEPP-2000 e^+e^- collider. We have measured the cross section for this process and for the four
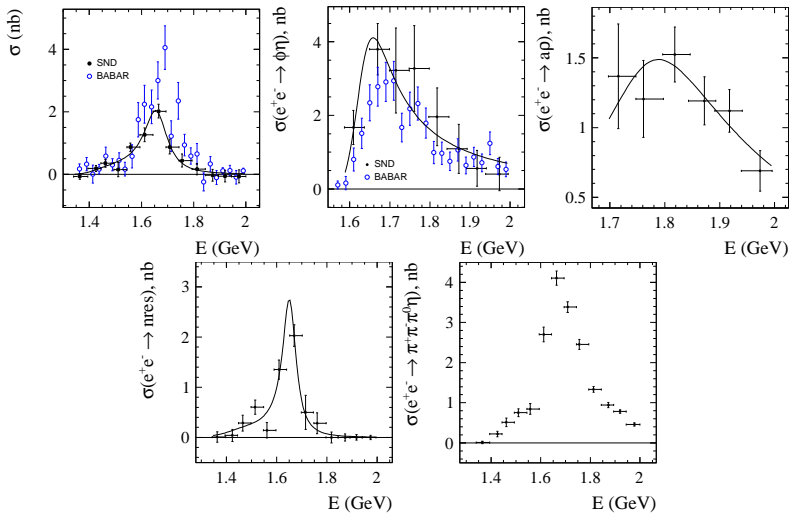
Figure 5. The cross sections measured in this work (filled circles) and in the *BABAR* experiment (open circles). The curve is the result of the fit described in the text. The errors of the SND data are statistical and systematic, combined in quadrature.

intermediate states in the c.m. energy range 1.34–2.00 GeV. The measured cross sections are well described in the vector meson dominance model.

References

[1] V. P. Druzhinin *et al.* (*SND* Collaboration), EPJ Web Conf. **130**, 05004 (2016) [arXiv:1609.01040 [hep-ex]]

[2] M. N. Achasov *et al.* (*SND* Collaboration), Phys. Rev. D **94**, 092002 (2016)

[3] B. Aubert *et al.* (*BABAR* Collaboration), Phys. Rev. D **76**, 092005 (2007)

[4] B. Aubert *et al.* (*BABAR* Collaboration), Phys. Rev. D **77**, 092002 (2008)

[5] R. R. Akhmetshin *et al.* (*CMD-3* Collaboration), Phys. Lett. B **773**, 150 (2017)

[6] M. N. Achasov *et al.*, Nucl. Instrum. Methods Phys. Res., Sect. A **598**, 31 (2009); V. M. Aulchenko *et al.*, *ibid.* **598**, 102 (2009); A. Yu. Barnyakov *et al.*, *ibid.* **598**, 163 (2009); V. M. Aulchenko *et al.*, *ibid.* **598**, 340 (2009)

[7] A. Romanov *et al.*, in *Proceedings of Particle Accelerator Conference PAC 2013*, Pasadena, CA USA, p. 14, (2013)

[8] E. A. Kuraev and V. S. Fadin, Yad. Fiz. **41**, 733 (1985) [Sov. J. Nucl. Phys. **41**, 466 (1985)]

[9] S. Agostinelli *et al.*, Nucl. Instrum. Methods Phys. Res., Sect. A **506**, 250 (2003)

[10] S. Jadach, W. Placzek, and B. F. L. Ward, Phys. Lett. B **390**, 298 (1997)

[11] K. A. Olive *et al.* (Particle Data Group), Chin. Phys. C **38**, 090001 (2014)